



Characterization of spontaneous magnetic signals for residual stress in plasma transferred arc welding process

Zhengchun Qian¹ · Haihong Huang¹ · Lunwu Zhao¹ · Qingdi Ke¹ · Gang Han¹

Received: 5 February 2018 / Accepted: 23 October 2018 / Published online: 30 October 2018
© International Institute of Welding 2018

Abstract

The residual stress produced in plasma transferred arc welding (PTAW) has strong effects on the service performance of remanufacturing components. In this study, a novel non-destructive testing method based on spontaneous magnetic signals is used to characterize the residual stress in PTAW. Experimental results show that both magnetic signal tangential components $H_p(x)$ and normal components $H_p(y)$ can locate the high residual stress zones from the welded specimen. A new characteristic value H_p is proposed to reflect the residual stress distribution, and its average value H_{pa} is further calculated to quantify the residual stress level. The characteristic value H_{pa} increases exponentially with an increase in average residual stress σ_a paralleled to the cladding coating, whereas it decreases linearly perpendicular to the cladding coating. Except for the temperature gradients, the various phases with different material mechanical properties may lead to different volume shrinkage during cooling process, which is the possible reason underlying the high residual stress and large magnetic field at heat affected zone (HAZ).

Keywords Plasma transferred arc welding · Residual stress · Spontaneous magnetic signals · Magnetic memory method

1 Introduction

Plasma transferred arc welding (PTAW) is commonly employed to prepare a cladding coating on a metallic substrate, which exhibits special advantages including low dilution rate, intensive energy density, and high deposition speed. The metal powders are melted immediately when they pass through the plasma beam between positive and negative electrode. PTAW has been widely applied to the equipment remanufacturing of petrochemical industry, engineering machinery, and mining machinery [1], since the deposition of metal powders over the damage region can greatly improve the wear resistance and corrosion resistance of components. However, during PTAW, the residual stress presented at welding area and heat affected zone (HAZ) is complicated and inevitable attributed to the combined actions of plastic deformation, temperature gradients, and metallurgical changes [2]. The residual

stress can greatly reduce the fatigue strength, induce crack initiation and even lead to serious accident, which affects the service performance and life of ferromagnetic structural components [3]. Therefore, how to evaluate the residual stress rapidly and accurately has been the key to guaranteeing the quality of components repaired by PTAW.

At present, the hole-drilling and X-ray diffraction (XRD) are two common detection methods to evaluate the residual stress of a component. However, the hole-drilling method can lead to irreversible destruction; and the XRD method is also confined in high cost, low efficiency, and radiation hazard. As a kind of novel non-destructive testing technique, magnetic memory method (MMM) has attracted considerable attention worldwide due to its special advantages of simple operation, high speed, and easy online testing. Previous researches [4–6] show that MMM can determine the location of stress concentration in ferromagnetic materials based on spontaneous magnetic signals without a specialized excitation device. The fundamental of MMM is based on the force/magnetism coupling effect. When the ferromagnetic materials are subjected to stress, the orientation and distribution of magnetic domains will change under geomagnetic field, which leads to the variations in spontaneous magnetization. Consequently, in ideal condition, the leakage magnetic field is generated in the stress concentration zones, where tangential components $H_p(x)$ reach the maximum value and normal components $H_p(y)$ change

Recommended for publication by Commission V - NDT and Quality Assurance of Welded Products

✉ Haihong Huang
huanghaihong@hfut.edu.cn

¹ School of Mechanical Engineering, Hefei University of Technology, Hefei 230009, China

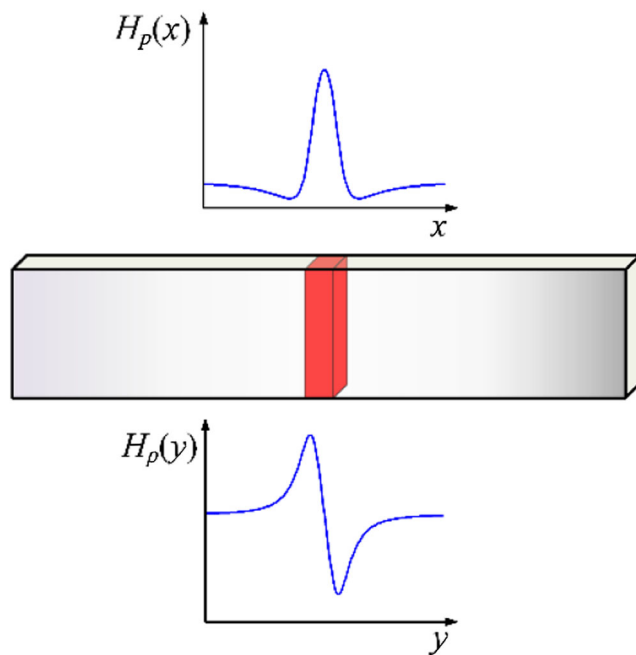


Fig. 1 Spontaneous magnetic signals of stress concentration zone

polarity and have a zero value [7], as shown in Fig. 1. It indicates that the spontaneous magnetic signals have the potential to evaluate the early damage degree and forecast the residual service life of ferromagnetic structural components [8].

The considerable researches on welding residual stress have been carried out by spontaneous magnetic signals. Qi et al. [9] investigated the stress distribution of welded seam on the CCSB ship plate by using MMM and the results showed that the region with high residual stress can be located rapidly. Liang et al. [10] evaluated the residual stress qualitatively dependent on the gradient of magnetic signal $H_p(y)$ perpendicular to welded seam. Dubov et al. [11, 12] assessed the stress state of welded joints by using MMM because they recognized that the stress concentration zones are sources of which pipeline damage emerges and develops [13]. In addition, a series of welding researches conducted by Roskosz showed that the non-uniform distribution of welded residual stresses resulted in variations in magnetic signals [14], which could be used to assess the level of residual stress in welded seams [15]. Except for the welded seams, Liu et al. [16] also evaluated the residual stress in laser cladding coating. It was showed that the slope of magnetic signal $H_p(y)$ increased with an increase in stress, but decreased when stress approached

Table 1 Chemical composition of Ni60 feed powder (wt%)

Material	C	Cr	Si	B	Fe	Ni
Ni60	0.6~1.0	14~17	3.0~4.5	2.5~4.5	≤15	Bal.

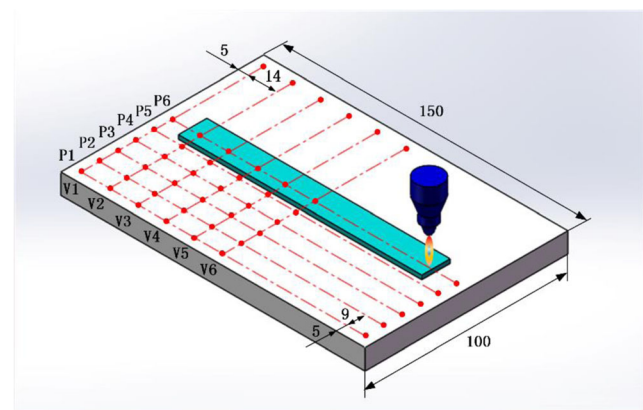


Fig. 2 Size and location of PTAW cladding coating and scanning lines

the yield strength. Similarly, Huang et al. [17] detected the stress of PTAW cladding coating and found that the gradient of magnetic signal K increased with an increase in stress at the elastic stage, while it decreased when deformation entered the plastic stage. Besides, the hysteresis curves of PTAW cladding coating were also analyzed to explain the change mechanism of magnetic signals with stress [18]. Previous studies of MMM primarily focused on the stress evaluation of welded seam and cladding coating, but rarely addressed HAZ. In fact, residual stress can also occur at HAZ where the temperature exceeds the critical values for phase transformations [2]; and the stress concentration zones are usually the locations of defects or material properties degradation [19]. Accordingly, residual stress evaluation for HAZ is an urgent problem.

In this paper, the variations of spontaneous magnetic signal tangential components $H_p(x)$ and normal components $H_p(y)$ are studied to reflect the residual stress in PTAW cladding coating and HAZ. The distribution and level of residual stress are further characterized by new proposed spatial magnetic signal characteristic value H_p and its average value H_{pa} , respectively. In order to validate the reliability of magnetic method applied, the residual stress in the welded specimen is analyzed by XRD, and microstructure and microhardness are also investigated. Based on this, the generation mechanisms of high residual stress and large magnetic field at HAZ are finally illuminated to provide guidance for the quality control of a ferromagnetic components repaired by PTAW.

Table 2 Processing parameters of PTAW

Parameters	Unit	Value
Plasma arc current	A	100
Plasma arc voltage	V	26
Welding speed	mm/min	65
Powder feeding rate	g/min	18

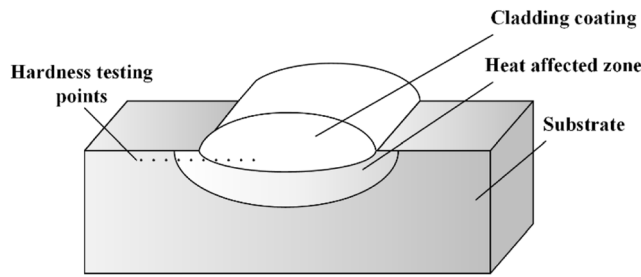


Fig. 3 Schematic diagram of cross section

2 Experiment

2.1 Specimen preparation

The ferromagnetic Q345 structural steel with dimensions of 150 × 100 × 10 mm is chosen as the substrate of PTAW due to its good mechanical and welding properties. Nickel based self-fluxing alloy (Ni60) is used as feed powder whose chemical composition is shown in Table 1. The size and location of PTAW cladding coating is given in Fig. 2. Since the cladding coating is centrosymmetric about the midpoint of specimen, only one side of residual stress distribution on the specimen is investigated. Six scanning lines, marked by P1–P6, are arranged along the cladding coating, while other six scanning lines, marked by V1–V6, are perpendicular to the cladding coating. All these scanning lines have thirty-six intersection points.

2.2 Testing method

To eliminate the effect of mechanical processing and transportation on the initial magnetic signals, the substrate was polished and demagnetized before PTAW. Then, the substrate was placed on a non-magnetic material platform along the South-North direction. During the detection process, the initial magnetic signals were measured on each scanning line by TSC-2M-8 device. The measurement system was made by the Energodiagnostika Co. Ltd. The probe with a 1 A/m sensitivity based on Hall sensor was gripped on a non-ferromagnetic scanning device, and was placed vertical to the surface of specimen with a lift-off value of 5 mm and horizontal movement speed of 8 mm/s. The probe can collect the magnetic signal tangential components and normal components simultaneously with a scanning increment of 1 mm along the scanning direction. The initial stress states in the 36 intersection points were also detected by XRD before PTAW.

Table 3 Specification of MMM measurement system

Parameters	Unit	Value
Sensitivity	A/m	1
Lift-off	mm	5
Movement speed	mm/s	8
Scanning increment	mm	1

Table 4 Specification of XRD measurement system

Parameters	Unit	Value
Accuracy	MPa	± 8
Penetration depth	μm	30
Measurement point size	mm	0.5
Testing time	min	3

The cladding coating was deposited by PTAW on the substrate after aforementioned detection procedure. The main processing parameters of PTAW are given in Table 2. The dimensions of the cladding coating are 120 × 14 × 4 mm without defects of porosity and cracking. Repeated as aforementioned detection method and procedure, the residual magnetic signals and residual stress states were also measured after the specimen was sufficient cooling. Then, the specimen was sectioned along the V6 scanning line and the cross section is shown in Fig. 3. The microstructures of cladding coating, HAZ, and substrate were observed respectively by metallographic microscope. Before examination, the cross section was polished and etched in 4% nital. The microhardness was also measured along the testing points by a low load Vickers hardness tester with hardness gradient test method as shown in Fig. 3. In the experiment, the specifications about the measurement system of MMM, XRD, and microhardness are listed in Tables 3, 4, and 5 respectively.

2.3 Data processing

As a kind of spontaneous weak magnetic signals, the measurement accuracy of MMM is easily interfered by external environment and the data fluctuation may occur during the testing. In order to reduce the testing error, the magnetic signals on each scanning line were collected repeatedly at three different times and their average value was considered as the final result. The scattering of the data was characterized by standard error bars. It can be found that all the testing errors are very small, which indicates that the magnetic signals are stable and available to the further analysis.

In this paper, the variations of magnetic signal tangential components $H_p(x)$ and normal components $H_p(y)$ are respectively given as:

$$H_p(x) = H_{p2}(x) - H_{p1}(x) \tag{1}$$

$$H_p(y) = H_{p2}(y) - H_{p1}(y) \tag{2}$$

Table 5 Specification of microhardness measurement system

Parameters	Unit	Value
Sensitivity	HV	1
Applied load	N	9.8
Loading time	s	15
Dwell time	s	10

where $H_{p1}(x)$ and $H_{p2}(x)$ denote the collected magnetic signals tangential components before and after PTAW, respectively; and $H_{p1}(y)$ and $H_{p2}(y)$ denote the collected magnetic signals normal components before and after PTAW, respectively. Actually, the main interest in this paper is on the change laws of magnetic signals under the effect of PTAW, rather than the intensity of magnetic signals collected before or after PTAW. Therefore, we pay more attention to researching the differential value of magnetic signals induced by PTAW in the following sections.

3 Results

3.1 Magnetic signals parallel to the cladding coating

Based on the aforementioned data processing, the magnetic signals on lines P1–P6 parallel to the cladding coating are given in Fig. 4. The magnetic signal tangential components $H_p(x)$ formed U-shaped curves as shown in Fig. 4a. From lines P1 to P5, the valley value of $H_p(x)$ increases with decreasing distance from the cladding coating. Similarly, it can be seen from Fig. 4b that the normal component curves rotate clockwise, which means that the intensity of $H_p(y)$ and its gradient absolute value increase with decreasing distance from the cladding coating as well. However, both the valley value of $H_p(x)$ and the gradient absolute value of $H_p(y)$ on line P6 start to decrease compared with other scanning lines. It indicates that the magnetic signals on cladding coating are smaller than that on HAZ.

In addition, both valley value of $H_p(x)$ and zero value of $H_p(y)$ are located at the range of about 80 to 100 mm. Based on the evaluation criteria from Fig. 1 and Ref. [7], we can deduce that high residual stress also mainly concentrates in this range. It is interesting that the high stress concentration zone deviates from the middle position of scanning lines. One of main mechanisms generating residual stress is temperature gradients [2]. Understanding the temperature distribution in PTAW process can be of great importance to study variations of magnetic signals and stress. At the beginning of PTAW, only a very

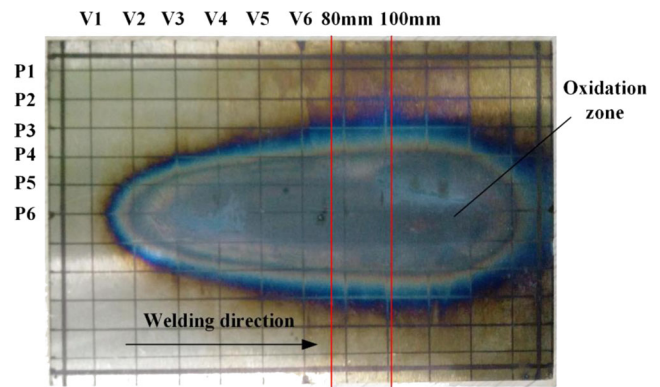


Fig. 5 Spindle shaped welding oxidation zone on the back of substrate

little heat is carried to the substrate because the fluctuations in powder delivery and the instability of plasma beam [20]. As the PTAW is going on, the heat increases continuously and sharp temperature gradient is present at the latter portion of specimen where the higher residual stress and wider welding oxidation zone appear. Therefore, the maximum width zone of welding oxidation is also located at the range of about 80 to 100 mm on the back of substrate as shown in Fig. 5. It indicates that the oxidation zone induced by high temperature can reflect the location of high residual stress and magnetic signal feature such as valley value of $H_p(x)$ or zero value of $H_p(y)$.

3.2 Magnetic signals perpendicular to the cladding coating

Analogously, the variations of magnetic signals perpendicular to the cladding coating are given in Fig. 6. The magnetic signal tangential components $H_p(x)$ on lines V2–V6 showed peaks-troughs in Fig. 6a. In order to better describe the variations of magnetic signals under the effect PTAW, the actual distribution of deposition track on specimen is displayed in Fig. 7. It can be seen that the cladding coating is located at the middle position of specimen and its width is about 14 mm. Based on this, the red dashed lines, which can represent the actual position and width of cladding coating, are marked in

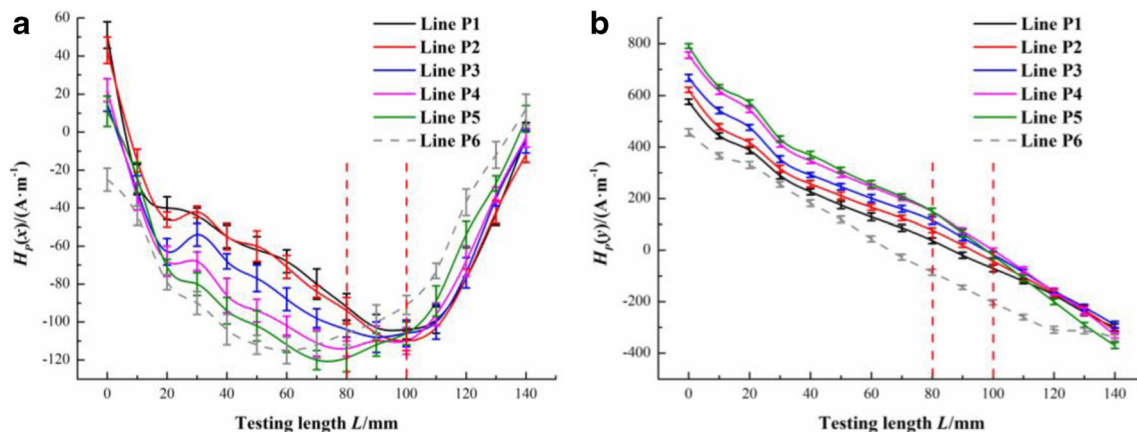


Fig. 4 Magnetic signals parallel to the cladding coating. **a** Tangential components $H_p(x)$. **b** Normal components $H_p(y)$

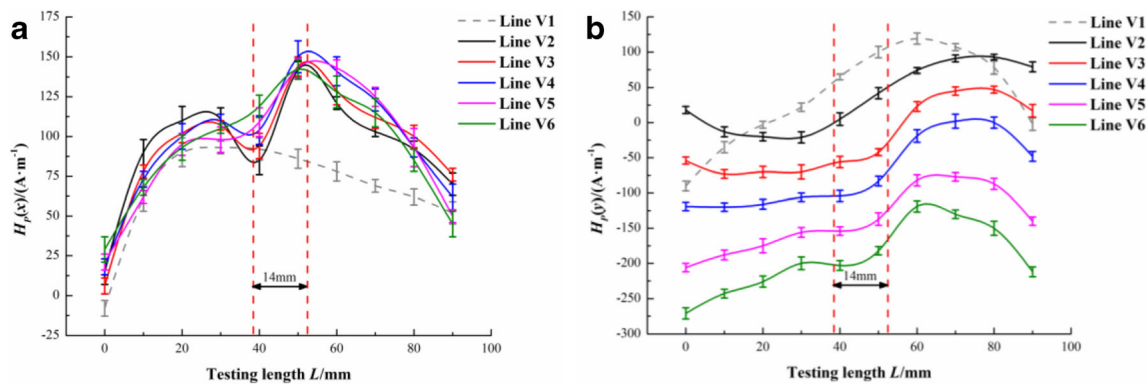


Fig. 6 Magnetic signals perpendicular to the cladding coating. **a** Tangential components $H_p(x)$. **b** Normal components $H_p(y)$

Fig. 6. It can be found that the overall trends of distance between peak and trough and its middle position are almost coincided with the width and position of cladding coating. In addition, it can be seen from Fig. 6b that the slopes of magnetic signal normal components $H_p(y)$ increase gradually when they enter the cladding coating zone, and reach the maximum at HAZ. Meanwhile, the overall $H_p(y)$ curves move down, which means that the overall intensity of magnetic signals increases along the deposition track movement direction. It is indicated that the residual stress on line V2 is the lowest because of low energy input at the beginning of PTAW as mentioned before. On the contrary, the residual stress on line V6 is the highest attributed to more energy input with the progress of PTAW. Furthermore, the variation of magnetic signals on line V1 without passing through the cladding coating is obvious different from other scanning lines. It is impossible to reflect the information about width and position of cladding coating only based on the detection result on line V1.

It is worth noting that the magnetic memory signals are susceptible to numerous interference factors which can bring substantial difficulties for signal feature extraction. The variations of real measured magnetic signals as shown in Fig. 6 are not in absolutely accordance with the ideal results in Fig. 1 or in ref. [7]. The tangential components $H_p(x)$ may only reach a maximum value at local high residual stress region rather than global area. And the zero-crossing position of normal components $H_p(y)$

may not have certain correlation with stress concentration [21]. It indicates that it is difficult to reflect the stress distribution by only two conventional characteristic values $H_p(x)$ or $H_p(y)$. We need to propose a new characteristic value to further characterize the residual stress of PTAW in the rest of paper.

3.3 Three-dimensional spatial magnetic signals

In order to better reflect the distribution of PTAW residual stress, the three-dimensional spatial magnetic signals are given as following:

$$H_p = \pm \sqrt{[H_{pp}(x)]^2 + [H_{pv}(x)]^2 + [(H_{pp}(y) + H_{pv}(y))/2]^2} \quad (3)$$

where $H_{pp}(x)$ and $H_{pp}(y)$ are respectively magnetic signal tangential components and normal components parallel to the cladding coating. $H_{pv}(x)$ and $H_{pv}(y)$ are respectively magnetic signal tangential components and normal components perpendicular to cladding coating. The projection of spatial magnetic signal characteristic value H_p in three-dimensional Cartesian coordinate

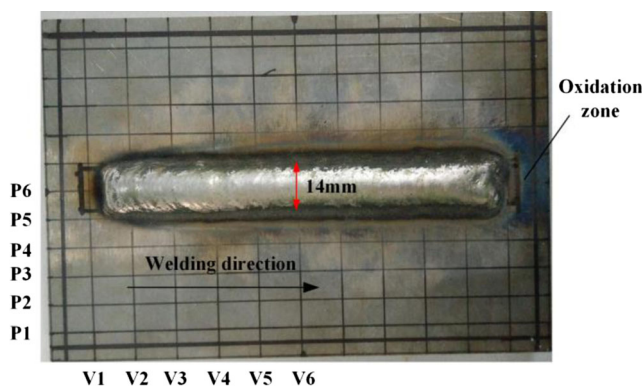


Fig. 7 Width and position of PTAW cladding coating

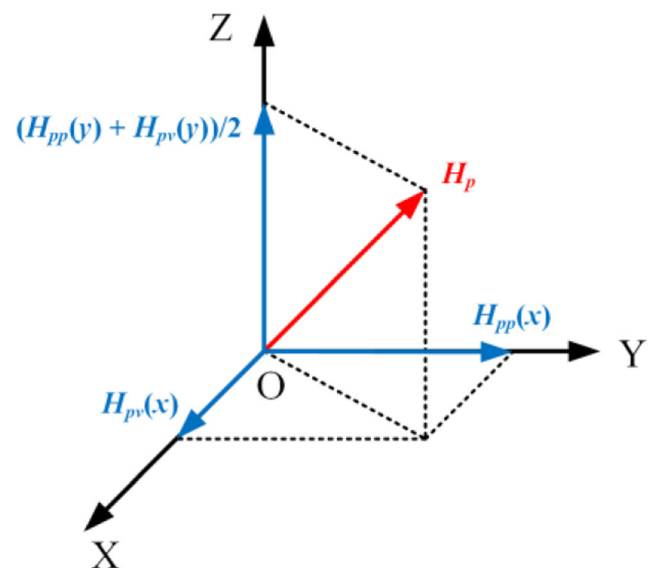


Fig. 8 The projection of H_p in three-dimensional Cartesian coordinate system

system is shown in Fig. 8. The average value of $H_{pp}(y)$ and $H_{pv}(y)$ is considered as component of Z axis. The characteristic value H_p is assigned positive when it points to the positive direction of Z axis, while negative when points to the opposite direction. The characteristic values H_p at thirty-six intersection points are calculated and their distribution nephogram is given in Fig. 9 based on two-dimensional discrete interpolation method.

For the scanning lines parallel to the cladding coating, it can be observed from Fig. 9 that the gradient of spatial magnetic signals H_p on line P5 reaches the maximum along the arrow marked at HAZ; however, the intensity of spatial magnetic signals H_p decreases. Based on Ref. [22, 23], the specimen can be considered as a whole piece of magnetic block with positive and negative magnetic pole distributed on the two sides of specimen respectively. The schematic diagram of magnetic induction line distribution on the surface of specimen in PTAW is shown in Fig. 10. A large number of magnetic induction lines leak out from the left edge of specimen where the larger magnetic flux density is present. Therefore, the intensity of spontaneous magnetic field decreases when the magnetic induction lines are far away from the left edge of specimen. For the scanning lines perpendicular to the cladding coating, the intensity of spatial magnetic signals H_p along lines V1–V6 also reaches the maximum at HAZ. As well known, the residual stress is mainly concentrated near the interface of coating [24]. Therefore, the dramatic increase of spatial magnetic signals H_p near coating may be induced by the high residual stress in HAZ.

4 Analysis and discussion

4.1 XRD method

In order to verify the reliability of MMM, the spatial magnetic signals H_p are compared with the residual stress measured by XRD method. The detection results parallel to the cladding

Fig. 9 Distribution nephogram of three-dimensional spatial magnetic signals H_p

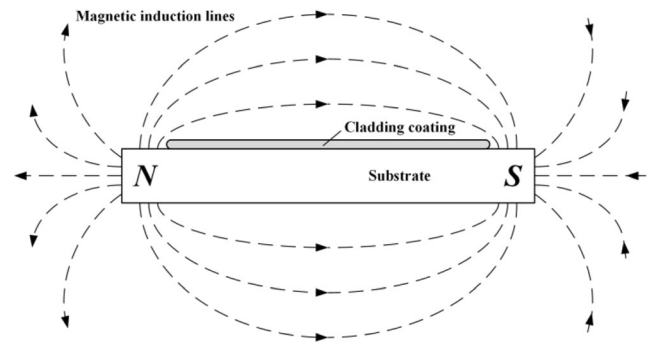
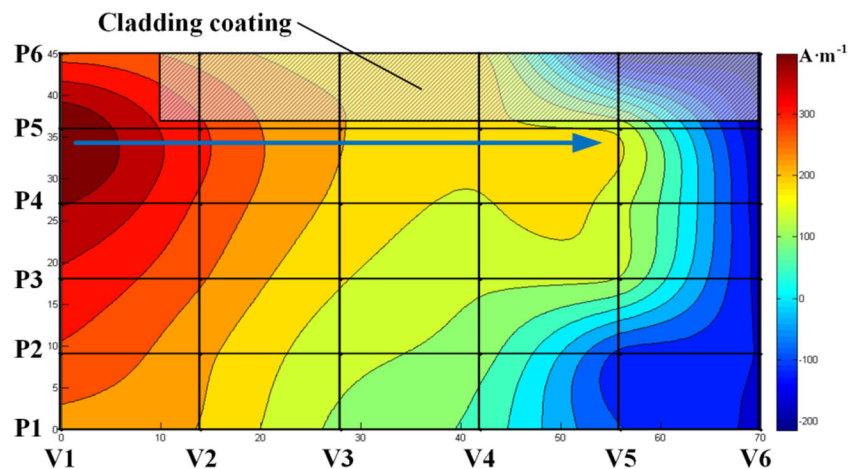


Fig. 10 Schematic diagram of magnetic induction line distribution on the surface of specimen

coating are shown in Fig. 11. The XRD residual stress shows increasing trend on lines P1–P6 because more heat and higher temperature gradient are concentrated at the latter portion of testing line as the plasma beam moves forward during the PTAW process. However, the spatial magnetic signal value H_p on lines P1–P6 shows decreasing trend. The phenomenon has been explained in Section 3.3 by assuming the specimen as a magnetic block, which leads to a large amount of magnetic flux density concentrated at the front portion of testing line. The detection results perpendicular to the cladding coating are also given in Fig. 12. It can be found that the maximum values of residual stress and spatial magnetic signals H_p are both located at the line P5 position (i.e., HAZ next to the cladding coating) except for V6. The individual detection result does not follow the change law may be due to the signal interference by some external factors [25]. And the deviation of individual detection result may not affect the overall variation trends of residual stress or magnetic signals.

According to the magnetomechanical model [26], the variation of stress can lead to change of spontaneous magnetization. Some studies have been carried out to establish the quantitative relationship between stress and magnetic signals successfully [27, 28]. Furthermore, it seems that the spatial magnetic signal is relevant to residual stress in PTAW based on aforementioned analysis. The average values of XRD residual

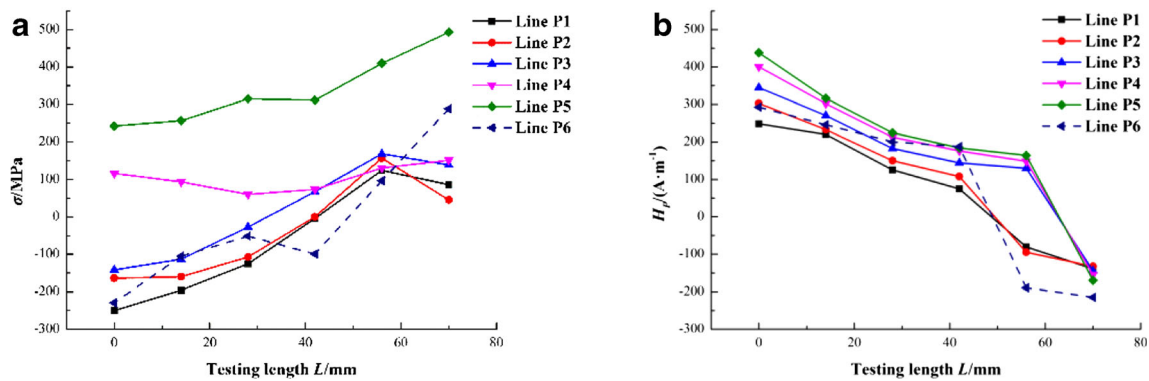


Fig. 11 Detection results parallel to the cladding coating. a XRD residual stress. b Spatial magnetic signals

stress σ_a and spatial magnetic signals H_{pa} on each scanning line are defined as follows, respectively:

$$\sigma_a = \frac{1}{I} \sum_{i=1}^I \sigma_i \tag{4}$$

$$H_{pa} = \frac{1}{I} \sum_{i=1}^I H_{pi} \tag{5}$$

where σ_i is the residual stress of the i th data point measured by XRD, H_{pi} is the spatial magnetic signal of the i th data point calculated based on Eq. (3), and $I=6$ is the number of data points. The variations of average values of XRD residual stress σ_a and spatial magnetic signals H_{pa} on each scanning line are plotted in Fig. 13. It is believed that H_{pa} parallel to the cladding coating is positively related to σ_a except for line P6, while H_{pa} perpendicular to the cladding coating is negatively related to σ_a . One key issue on the MMM applied to PTAW is to establish the quantitative relationship between the residual stress and magnetic signal characteristic value. As shown in Fig. 14a, an approximate exponential relationship is found between σ_a and H_{pa} parallel to the cladding coating, which can be fitted by the following exponential fitting equation:

$$H_{pa} = c_1 + a_1 \times \exp(b_1 \sigma_a) \tag{6}$$

where a_1 , b_1 , and c_1 are constant values related with processing parameters of PTAW. In this experiment, a_1 is -55.368 , b_1 is $-$

0.013 , and c_1 is 194.776 ; and R^2 (adjusted deviate square) is 0.980 . It can be found that the growth rate of magnetic signals decreases with an increase in residual stress when approaching to the line P5 position. It is responsible for the enormous quantitatively differences between residual stress and magnetic signals especially for line P5 in Fig. 11. For testing perpendicular to the cladding coating, a linear relationship between σ_a and H_{pa} is plotted in Fig. 14b and the fitting equation is listed as follows:

$$H_{pa} = a_2 + b_2 \times \sigma_a \tag{7}$$

where a_2 and b_2 are constant values also affected by processing parameters of PTAW. In this equation, a_2 is 218.587 , b_2 is -1.542 , and R^2 is 0.915 . Good agreement is achieved between the spatial magnetic signals and residual stress measured by XRD, which shows that characteristic value H_p and its average value H_{pa} have the capacity to reflect the distribution and level of residual stress in PTAW, respectively.

4.2 Microstructure

The microstructures of cladding coating, HAZ, and substrate are observed respectively to explore the effect of PTAW on distribution of spontaneous magnetic signals and residual stress. When a high energy plasma beam irradiates the molten pool in PTAW, the temperature gradient between the bottom of the molten pool and

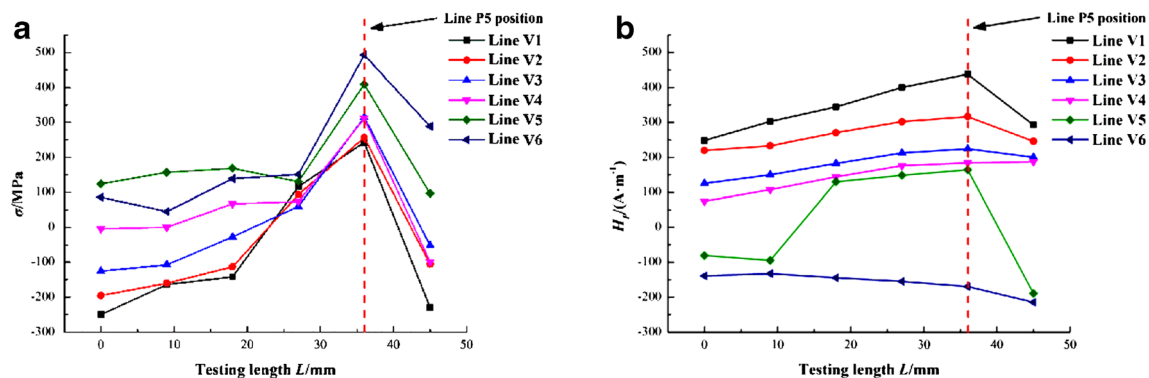


Fig. 12 Detection results perpendicular to the cladding coating. a XRD residual stress. b Spatial magnetic signals

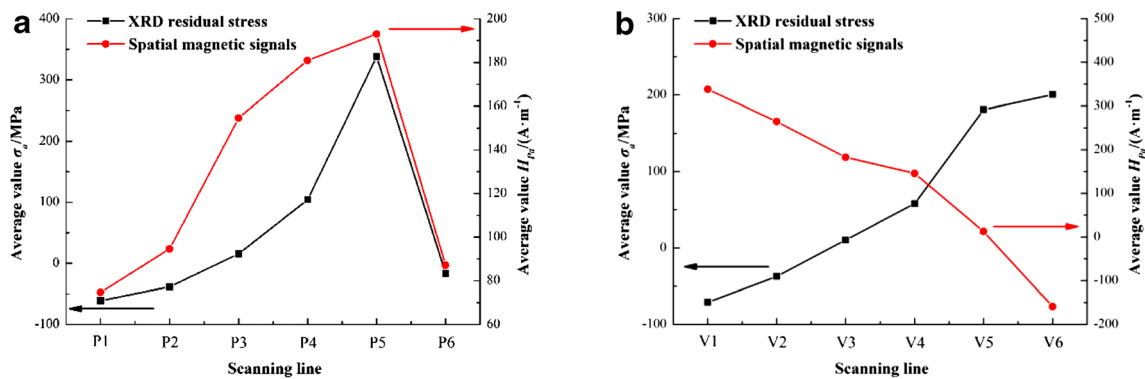


Fig. 13 Variations of σ_a and H_{pa} . **a** Parallel to the cladding coating. **b** Perpendicular to the cladding coating

the surface provides a driving force for the growth of the grain. The crystal development of austenite, considered as the initial phase, is significantly promoted because the wide subcooled region in front of liquid-solid interface brings the sufficient time for the grain growth [29]. However, when the plasma beam moves out of the molten pool and the temperature is lower than A_{r3} , the primary austenite phase partially transforms into ferrite or pearlite due to the high solidification rates [30]. Finally, it can be seen from Fig. 15a that the obvious dendrites with residual austenite, acicular ferrite, and Widmanstatten ferrite are present in the cladding coating at room temperature. Besides, a large amount of carbide and boride with high hardness are also precipitated, which can help to improve the abrasive resistance of coating. As a kind of paramagnetic material, austenite can hardly be magnetized spontaneously. Therefore, the magnetic signal intensity of cladding coating contained partial austenitic structure is weaker than that of HAZ. This is responsible for not only the reduction of the valley value of $H_p(x)$ and the gradient absolute value of $H_p(y)$ on line P6 as shown in Fig. 4, but also the abrupt reduction of spatial magnetic signal H_p at line P6 position as shown in Fig. 12.

The HAZ can be classified as overheated zone and recrystallization zone. Their microstructure can be seen in Fig. 15b, c, respectively. We can find that the grain coarsening occurred in Fig. 15b where a large amount of pearlite is present in this area due to element diffusion of carbon and alloy [30]. Besides, a

certain amount of bainite appears attributed to high temperature and cooling rate. In Fig. 15c far away from heat source, the finer grains can be observed at the recrystallization zone composed of pearlite and ferrite. During the cooling process, the non-uniform shrinkage effect of weld seam occurs due to surrounding temperature gradients. Besides, the volumetric change at microscale is induced by these phase transformation in HAZ. They are both responsible for the increment of strain and residual stress. Based on the magnetomechanical effect, the residual stress in HAZ can lead to the spontaneous magnetic signals. It explains the distortion of magnetic signal components and larger spatial magnetic signals at HAZ as mentioned before.

The structure of substrate far away from HAZ contains ferrite and pearlite grains as shown in Fig. 15d, which is identical with the microstructure in the initial material before PATW. The residual stress in the substrate remains at the lower level because no phase transformation occurs.

4.3 Microhardness

The variations of magnetic signals and residual stress in PTAW are both related with metallographic structure change based on aforementioned analysis. As a significant evaluation indicator for welding quality, the microhardness is also strongly dependent on the metallographic structure. In order to better understand the

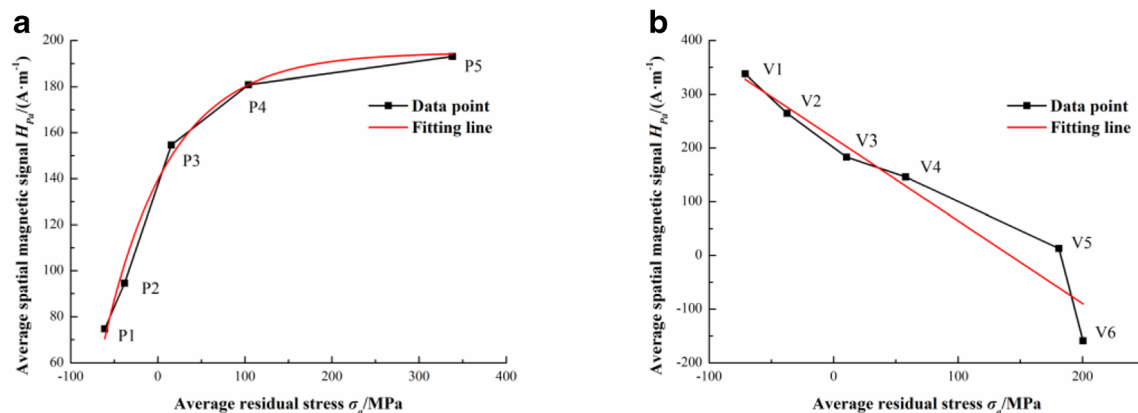
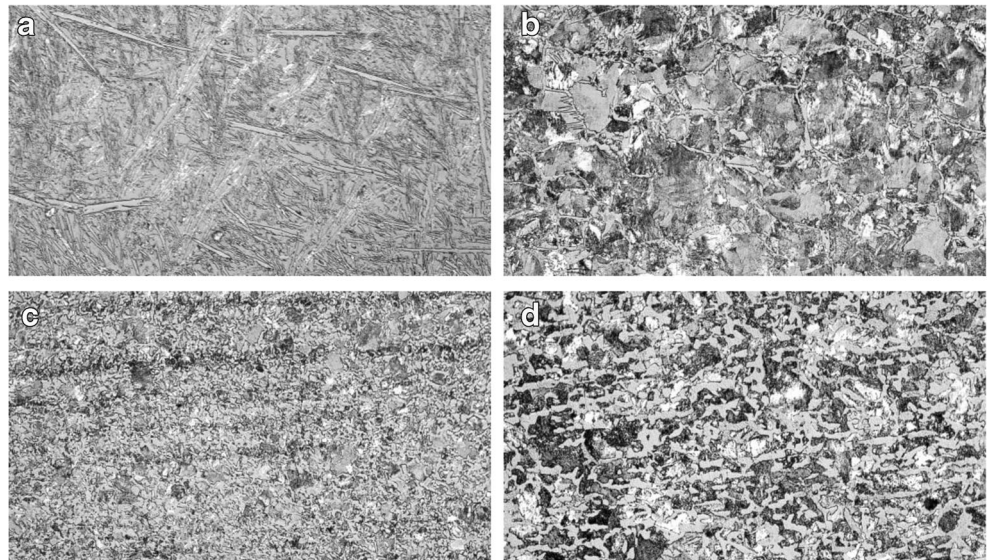


Fig. 14 Relationship between σ_a and H_{pa} . **a** Parallel to the cladding coating. **b** Perpendicular to the cladding coating

Fig. 15 Microstructure of PTAW specimen. **a** Cladding coating. **b** Overheated zone. **c** Recrystallization zone. **d** Substrate, magnification $\times 200$



change mechanism of magnetic signals and residual stress, it is useful to research the distribution of microhardness near fusion line and the testing results are shown in Fig. 16. The zero value position at abscissa axis corresponds to the fusion line. The negative value at abscissa axis represents cladding coating zone while positive value represents HAZ and substrate zones. The hardness of cladding coating is 600–700 HV, which shows great abrasive resistance due to the strengthening phase of carbide or boride dispersed in the Ni based alloy. When crossed the fusion line and entered the HAZ and substrate, the hardness reduces sharply to 250–300 HV because a large amount of pearlite and ferrite whose hardness is lower than strengthening phase appears. The rapid decrease in hardness from cladding coating into HAZ and substrate indicates that various phases exist at interface. The various phases with different material mechanical properties may lead to different volume shrinkage during cooling process, which is responsible for the high strain or stress concentrated near the bonding interface. Based on the magnetomechanical effect, the

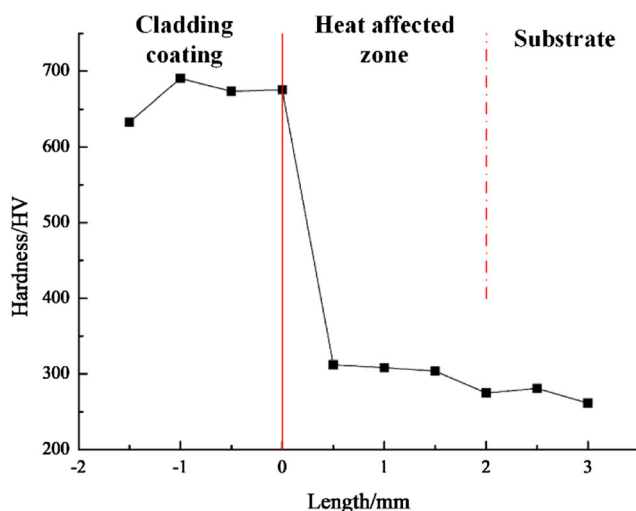


Fig. 16 Microhardness near fusion line

magnetic signal characteristic values H_p and H_{pa} also reach the maximum near interface as shown in Figs. 12b and 13a.

5 Conclusions

In this paper, a novel magnetic non-destructive testing method based on spontaneous magnetic signals is used to characterize the residual stress in PTAW. And this MMM technique can potentially replace the existing destructive methods of residual stress determination and contribute to the remanufacturing repair quality evaluation during PTAW. The major findings of the presented work are listed as follows:

1. Both magnetic signal tangential components $H_p(x)$ and normal components $H_p(y)$ can locate the high residual stress zones. And the amplitude of $H_p(x)$ and slope of $H_p(y)$ can determine the location and size of cladding coating.
2. The new proposed characteristic value H_p and its average value H_{pa} have the capacity to reflect the distribution and level of residual stress very well. The characteristic value H_{pa} increases exponentially with an increase in average residual stress σ_a paralleled to the cladding coating, whereas it decreases linearly perpendicular to the cladding coating.
3. The MMM can characterize the distribution and level of residual stress rapidly. Compared with other non-destructive testing methods, the MMM has the maximum measuring velocity of up to several meters per second [31] without concerning surface preparation [15]. Based on the horizontal movement speed of probe and the length of scanning line in this experiment, it only takes several minutes to collect all the magnetic signal data.
4. Various phases exist at different zones of specimen during the PTAW cooling process and thus the rapid decrease in hardness from cladding coating into HAZ occurs. Except

for the temperature gradients, the various phases with different material mechanical properties may lead to different volume shrinkage during cooling process, which is the possible reason underlying the high residual stress and large magnetic field at HAZ.

- Although the level of residual stress in HAZ may be different in various coating materials such as Ni, Fe, Co-based alloy, we can believe that these overall variation trends or distributions of residual stress are the same because the phase transformation always occurs at HAZ. Therefore, the MMM technique has a wide applicability to characterize the residual stress in PTAW.

Acknowledgements This work is financially supported by the National Natural Science Foundation of China (Grant Nos. 51675155, 51635010 and 51722502).

References

- Deng DW, Chen R, Zhang HC (2013) Present status and development tendency of plasma transferred arc welding [J]. *J Mech Eng* 49(7):106–112
- Yelbay HI, Cam I, Gür CH (2010) Non-destructive determination of residual stress state in steel weldments by magnetic Barkhausen noise technique [J]. *NDT&E Int* 43:29–33
- Dong LH, Wang Y, Guo WL (2014) Stress measuring techniques and applications in remanufacturing field [M]. National Defense Industry Press, Beijing
- Wang W, Yi SC, Su SQ (2016) Experimental investigation of stress and damage characterization of steel beam buckling using magnetic memory signals [J]. *Struct Design Tall Spec Build* 25(11):505–518
- Li HM, Chen ZM (2016) Quantitative analysis of the relationship between non-uniform stresses and residual magnetizations under geomagnetic fields [J]. *AIP Adv* 6(7):401–406
- Roskosz M, Bieniek M (2012) Evaluation of residual stress in ferromagnetic steels based on residual magnetic field measurements [J]. *NDT&E Int* 45:55–62
- Wang ZD, Gu Y, Wang YS (2012) A review of three magnetic NDT technologies [J]. *J Magn Magn Mater* 324(4):382–388
- Xu BS, Dong LH (2015) Metal magnetic memory testing method in remanufacturing quality control [M]. National Defense Industry Press, Beijing
- Qi X, Di S, Liu H et al (2012) Magnetic Barkhausen noise, metal magnetic memory testing and estimation of the ship plate welded structure stress [J]. *J Nondestruct Eval* 31:80–89
- Liang B, Gong JM, Wang HT, Ye C (2012) Evaluation of residual stresses in butt-welded joints by residual magnetic field measurements [J]. *Appl Mech Mater* 217–219:2427–2434
- Kolokolnikov S, Dubov A, Steklov O (2016) Assessment of welded joints stress-strain state inhomogeneity before and after post weld heat treatment based on the metal magnetic memory method [J]. *Welding in the World* 60:665–672
- Kolokolnikov S, Dubov A, Marchenkov A (2014) Determination of mechanical properties of metal of welded joints by strength parameters in the stress concentration zones detected by the metal magnetic memory method [J]. *Welding in the World* 58:699–706
- Dubov A, Kolokolnikov S (2010) Comprehensive diagnostics of parent metal and welded joints of steam pipeline bends [J]. *Welding in the World* 54(9–10):241–248
- Roskosz M (2016) Capabilities and limitations of using the residual magnetic field in NDT [C]. 19th World Conference on Non-Destructive Testing, Munich
- Roskosz M (2011) Metal magnetic memory testing of welded joints of ferritic and austenitic steels [J]. *NDT&E Int* 44:305–310
- Liu B, Chen SJ, Dong SY et al (2015) Stress measurement of laser cladded ferromagnetic coating with metal magnetic memory [J]. *Trans China Welding Inst* 36(8):23–26
- Huang HH, Han G, Yang C et al (2016) Stress evaluation of plasma sprayed cladding layer based on metal magnetic memory testing technology [J]. *J Mech Eng* 52(20):16–22
- Huang HH, Han G, Qian ZC et al (2017) Characterizing the magnetic memory signals on the surface of plasma transferred arc cladding coating under fatigue loads [J]. *J Magn Magn Mater* 443:281–286
- Dubov A, Dubov A, Kolokolnikov S (2014) Application of the metal magnetic memory method for detection of defects at the initial stage of their development for prevention of failures of power engineering welded steel structures and steam turbine parts [J]. *Welding in the World* 58:225–236
- Mandal S, Kumar S, Bhargava P, Preamsingh CH, Paul CP, Kukreja LM (2015) An experimental investigation and analysis of PTAW process [J]. *Mater Manuf Process* 30:1131–1137
- Zhang WM, Qiu ZC, Yuan JJ et al (2015) Discussion on stress quantitative evaluation using metal magnetic memory method [J]. *J Mech Eng* 51(8):9–13
- Li CC, Dong LH, Wang HD et al (2016) Metal magnetic memory technique used to predict the fatigue crack propagation behavior of 0.45% C steel [J]. *J Magn Magn Mater* 405:150–157
- Gao FM, Fan JC (2017) Research on the effect of remanence and the earth's magnetic field on tribo-magnetization phenomenon of ferromagnetic materials [J]. *Tribol Int* 109:165–173
- Xu L, Cao HJ, Liu HL et al (2017) Study on laser cladding remanufacturing process with FeCrNiCu alloy powder for thin-wall impeller blade [J]. *Int J Adv Manuf Technol* 90:1383–1392
- Ni C, Hua L, Wang XK (2018) Crack propagation analysis and fatigue life prediction for structural alloy steel based on metal magnetic memory testing [J]. *J Magn Magn Mater* 462:144–152
- Jiles DC (1995) Theory of the magnetomechanical effect [J]. *J Phys D Appl Phys* 28(8):1537–1546
- Shi PP, Jin K, Zheng XJ. A general nonlinear magnetomechanical model for ferromagnetic materials under a constant weak magnetic field [J]. *J Appl Phys*, 2016, 119: 145103–1–8
- Xu MX, Xu MQ, Li JW, Xing HY (2012) Using modified J-A model in MMM detection at elastic stress stage [J]. *Nondestruct Test Eva* 27(2):121–138
- Liu Y, Yang YQ, Wang D (2016) A study on the residual stress during selective laser melting (SLM) of metallic powder [J]. *Int J Adv Manuf Technol* 87:647–656
- Li JH, Lin DC (2015) Metallographic atlas of metallic materials [M]. China Machine Press, Beijing
- Huang HH, Qian ZC, Yang C et al (2017) Magnetic memory signals of ferromagnetic weldment induced by dynamic bending load [J]. *Nondestructive Testing and Nondestruct Test Eva* 32(2):166–184